Journal of Fluorescence, Vol. 13, No. 3, May 2003 (© 2003)

Silver Fractal-like Structures for Metal-Enhanced Fluorescence: Enhanced Fluorescence Intensities and Increased Probe Photostabilities

Chris D. Geddes,[1] Alexandr Parfenov,[2] David Roll,[3] Ignacy Gryczynski,[2] Joanna Malicka,[2] and Joseph R. Lakowicz[2,4]

Received January 11, 2003; revised January 20, 2003; accepted January 20, 2003

Substantial increases in fluorescence emission from fluorophore-protein–coated fractal-like silver structures have been observed. We review two methods for silver fractal structure preparation, which have been employed and studied. The first, a roughened silver electrode, typically yielded a 100-fold increase in fluorophore emission, and the second, silver fractal-like structures grown on glass between two silver electrodes, produced a ≈500-fold increase. In addition, significant increases in probe photostability were observed for probes coated on the silver fractal like structures. These results further serve to compliment our recent work on the effects of nobel metal particles with fluorophores, a relatively new phenomenon in fluorescence we have termed both "metal-enhanced fluorescence" [1] and "radiative decay engineering" [2,3]. These results are explained by the metallic surfaces modifying the radiative decay rate (Γ) of the fluorescent labels. We believe that this new silver-surface preparation, which results in ultrabright and photostable fluorophores, offers a new generic technology platform for increased fluorescence signal levels, with widespread potential applications to the analytical sciences, imaging, and medical diagnostics.

KEY WORDS: Metal-enhanced fluorescence; radiative decay engineering; fractal silver structures; increased photostabilities.

INTRODUCTION

We have recently reported the favorable effects obtained for fluorophores in close proximity to metallic particles and islands [1–9]. These effects include increased quantum yields, decreased lifetimes, increased photostability, and increased energy transfer. These effects are due to the interactions of excited-state fluorophores with the surface plasmon resonance (the oscillations of free electrons) on a metals surface [1,2,6,7]. These interactions result in increased rates of excitation, quenching, increased intensities, or quantum yield (Fig. 1). For the most favorable effect of enhanced fluorescence, we are mostly concerned with the important prospect of increasing the radiative decay rate (Γ) for fluorophores, which typically occurs when a fluorophore is positioned some ≈50–100 Å from an appropriately sized and shaped metallic particle. We have recently reviewed these criteria [1,2] and refer to the use of fluorophore-metal interactions as radiative decay engineering (RDE) [2,3] or metal-enhanced fluorescence (MEF) [1]. Interestingly, from Fig. 1 and Eqs. (1–4), when the radiative decay rate

[1]Center for Fluorescence Spectroscopy and Institute of Fluorescence, Medical Biotechnology Center, University of Maryland Biotechnology Institute, 725 West Lombard St, Baltimore, Maryland, 21201.
[2]University of Maryland School of Medicine, Center for Fluorescence Spectroscopy, Department of Biochemistry and Molecular Biology, 725 West Lombard St, Baltimore, Maryland 21201.
[3]Department of Chemistry, Roberts Wesleyan College, 2301 Westside Drive, Rochester, New York.
[4]To whom correspondence should be addressed. cfs@cfs.umbi.umd.edu

1053-0509/03/0500-0267/0

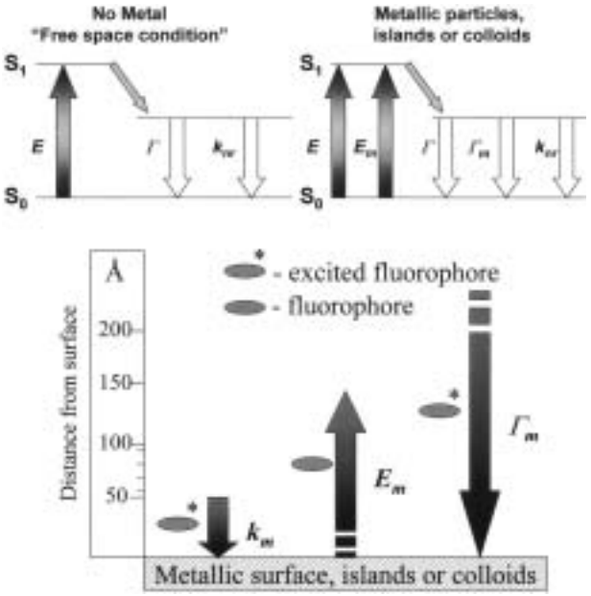

Fig. 1. Top, Classical Jablonski diagram for the free space condition and the modified form in the presence of metallic particles, islands or colloids. *E*-excitation. *Em*, Metal enhanced excitation rate; Γ*m*, radiative rate in the presence of metal. Bottom, Predicted distance dependencies for a metallic surface on the transitions of a fluorophore. The metallic surface can cause Förster-like quenching with a rate (*km*) can concentrate the incident field (*Em*) and can increase the radiative decay rate (Γ*m*).

(the spontaneous rate at which a fluorophore emits photons) is increased, the quantum yield increases while the lifetime decreases Eqs. (3,4). This is in stark contrast to the usual nonradiative rate modification observed in most fluorescence experiments, which typically results in the quantum yield and lifetime changing in unison.

For a typical fluorophore radiating into free space, the lifetime (τ_0) and quantum yield (Q_0) are given by:

$$\tau_0 = \frac{1}{k_{nr} + \Gamma} \tag{1}$$

$$Q_0 = \frac{\Gamma}{k_{nr} + \Gamma} \tag{2}$$

However, in the presence of metal (m) the lifetime (τ_m) and quantum yield (Q_m) can be given by

$$\tau_m = \frac{1}{k_{nr} + \Gamma + \Gamma_m} \tag{3}$$

$$Q_m = \frac{\Gamma + \Gamma_m}{k_{nr} + \Gamma + \Gamma_m} \tag{4}$$

In our previous work we considered several different silver surfaces for use in MEF. We considered silver island films, which are subwavelength-size silver particles deposited on glass by the citrate reduction of silver nitrate [3,4]. We also considered the immobilization of silver colloids onto a glass surface [5], as well as light-deposited silver [8], and the electroplating of silver from a pure water medium onto different substrates [9]. In all of our experiments to date we have considered both the method of silver deposition and the resultant effects on MEF. In these previous works it became apparent that for MEF to occur, there is a need to localize the fluorophore (or species of interest) in regions in close proximity to the silver surface. However, in many applications of fluorescence, it would be advantageous to have localized silver deposition for spatially selective analysis, such as for lab-on-a-chip technologies [10,11]. Localized silver colloid formation has been accomplished with reagents in laminar flow [12], by nanolithography [13,14], and by electroplating on insulators [15]. Given the extensive use of roughened silver electrodes for surface-enhanced Raman scattering (SERS) [16,17], we investigated their use for spatially selective MEF, given the typically high surface areas of fractal-like structures.

In our recent studies, we used two methods for producing silver fractal-like structures [18,19], but have not compared their respective merits for MEF. The first method involves using roughened silver electrodes, roughened by the passage of electrical current through the electrode [18]. This treatment resulted in the rapid formation of fractal-like structures on the surface of the electrode. The second method resulted in the fractal-like growth of silver structures on glass [19]. This was achieved by passing an electrical current between two electrodes, sandwiched between $SnCl_2$-treated glass slides. These freshly generated surfaces were allowed to bind a protein, human serum albumin (HSA), which had been labeled with indocyanine green (ICG) and fluorescein isothiocyanate (FITC). Indocyanine green and fluorescein were used because of their widespread use in medical testing, imaging, and sensing. We found dramatic increases in fluorescence emission intensities (>100 fold) using both procedures, which was accompanied by a substantial reduction in probe fluorescence lifetime. An increase in fluorescence quantum yield accompanied by a reduction in lifetime can only be explained by an increase in the radiate decay rate [Eqs. (3, 4)].

Finally, we investigated the potential use of chloride-dipped electrodes in MEF, which are widely used in SERS to enhance signal intensities [16,17]. Our findings show no enhancement in fluorescence emission after chloride dipping, which is consistent with MEF being a through-space phenomenon as compared to SERS, which conversely is thought to be a contact (or near contact) interaction with a metallic surface [20,21].

EXPERIMENTAL

ICG and HSA were obtained from Sigma (St. Louis, MO, USA) and used without further purification. Concentrations of ICG and HSA were determined using extinction coefficients of ε (780) = 130,000 cm^{-1} and ε (278) nm = 37,000 cm^{-1}, respectively.

For covalently labeling the FITC to HSA, 2 mg of HSA was dissolved in 1 ml of 0.1 *M* bicarbonate buffer (pH 9.2) and was mixed with 70 μL of fluorescein-5-isothiocyanate (FITC; Molecular Probes) solution in DMSO (2 mg FITC/200 μL DMSO). The reaction mixture was incubated for 2 h at room temperature, and the labeled protein was separated from the unreacted probe by passing over a Sephadex G-25 column equilibrated with 0.1 × PBS. The ratio of FITC-HSA in stock solution of labeled protein was determined by independent measurements of dye and protein concentrations, respectively. The amount of FITC was calculated using absorbance of FITC-HSA conjugates in 0.1 *M* bicarbonate buffer (pH 9.2) at 495 nm and molecular extinction coefficient of FITC ε(495 nm) = 76,000 $M^{-1}\cdot cm^{-1}$. The HSA concentration was determined by using Coommassie plus protein assay reagent (Pierce, IL, USA). For fluorescence measurements we used a sample with an average FITC-HSA ratio of 7. The advantages of an overlabeled protein for use in metal-enhanced fluorescence have recently been discussed [22].

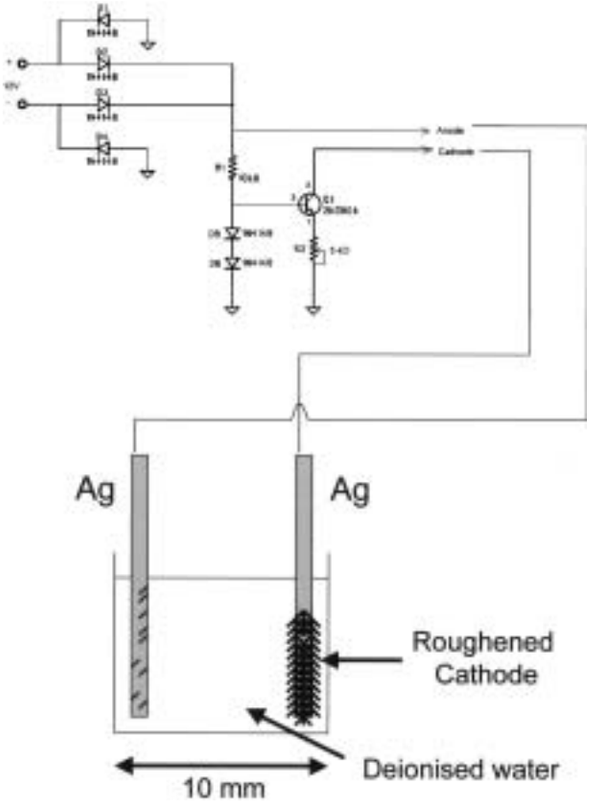

Fig. 2. Constant current circuit apparatus for silver fractal growth.

Roughened Silver Electrodes

The silver electrodes (Aldrich) had dimensions of 9 × 35 × 0.1 mm. A constant current generator circuit (Fig. 2) was used to supply 60 μA across the two electrodes for 10 min. The electrodes were separated by ≈10 mm. The space between the electrodes was filled with distilled water. Figure 3 shows the growth of the silver structures on the cathode.

Glass slides (Aldrich) were cleaned before use by immersion in 30% v/v H_2O_2 and 70% v/v H_2SO_4 for 48 h and then washed in distilled water. The glass slides were then used to sandwich the roughened silvered electrodes so as to keep the surfaces wet during measurements (Fig. 4).

Binding the ICG-HSA to the both the silver anode and cathode after electrolysis was accomplished by soaking the electrodes in a 30 μm ICG, 60 μ*M* HSA solution overnight, followed by rinsing with water to remove the unbound material. As a control sample, an unused silver electrode was also coated with ICG-HSA.

A roughened silver cathode was also dipped in 10^{-4} *M* NaCl for 1 h before being washed and then coated with ICG-HSA, so as to place our findings in context with the huge enhancements in Raman signals, typically obtained after chloride dipping the electrodes [16,17].

Silver Fractal-like Structures on Glass

Fractal-like silver structures were also generated on glass using two silver electrodes held between two glass microscope slides, Fig. 5. The electrodes were 10 × 35 × 0.1 mm, with about 20 mm between the two electrodes. Deionized water was placed between the slides. A direct current of 10 μA was passed between the electrodes for about 10 min, during which the voltage started near 5 V and decreased to 2 V. During the current flow, fractal silver structures grew on the cathode and then on the glass near the cathode (Fig. 5), thus producing silver structures on glass, compared to those described above on the silver electrodes. Similarly to the silver electrodes, the structures grew rapidly but appeared to twist as they grew. These structures are similar to those reported recently during electroplating of insulators [15]. In addition we found that dipping the slides in 0.001 mg/dl $SnCl_2$ for 30 min, *before electrolysis*, resulted in structures that were firmly bound to the glass during

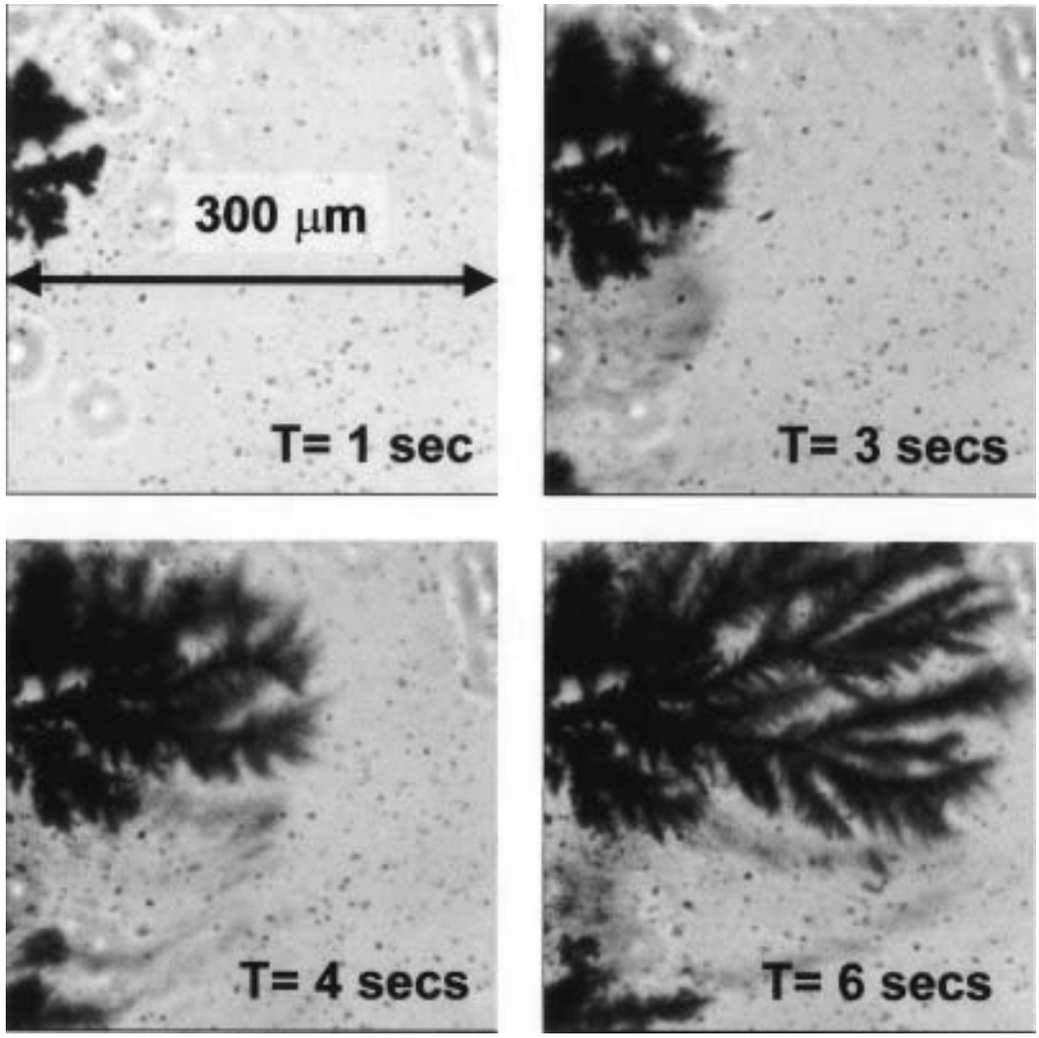

Fig. 3. Silver growth on the silver cathode as a function of time, visualized using transmitted light. This structure was characteristic of the whole electrode.

working. Without the $SnCl_2$, similar structures were formed but were partially removed during washing.

Following passage of the current, the silver structures on glass were soaked in 10 μ*M* FITC-HSA overnight at 4°C, which is thought to result in a monolayer of surface bound HSA [22,23].

Methods

Excitation and observation of the ICG-HSA coated roughened silver electrodes were made by the front face configuration (Fig. 4). Steady-state emission spectra were recorded using a SLM 8000 spectrofluorometer with excitation using a Spectra Physics Tsunami Ti:Sapphire laser in the CW (nonpulsed) mode, which was attenuated as required ≈200 mW 760 nm output.

The fractal-like silver structures on glass were observed using the apparatus shown in Fig. 5 (bottom). Bright-field and fluorescence images were obtained with a roper RLX-37 CCD camera. For fluorescence the 442 nm excitation was obtained from a HeCd laser, using about 2 mW. Emission was isolated with a 540 nm interference filter and a liquid cut-off filter at 525 nm. The liquid filter was an aqueous solution of CrO_4^{2-} and $Cr_2O_7^{2-}$, which completely eliminated scattered light and did not display autofluorescence.

Time-resolved intensity decays were measured in both the frequency domain (FD) and time-domain (TD—using

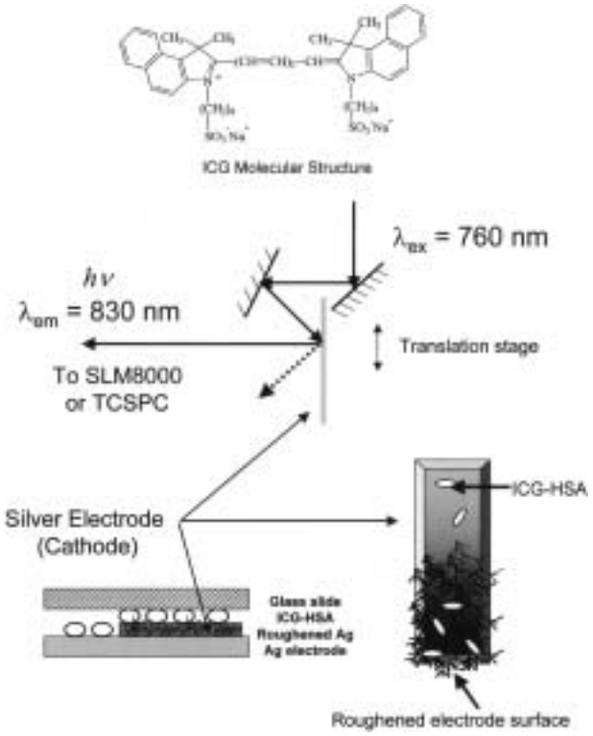

Fig. 4. Top, ICG molecular structure. Bottom, Experimental geometry used to study the roughened silver electrode.

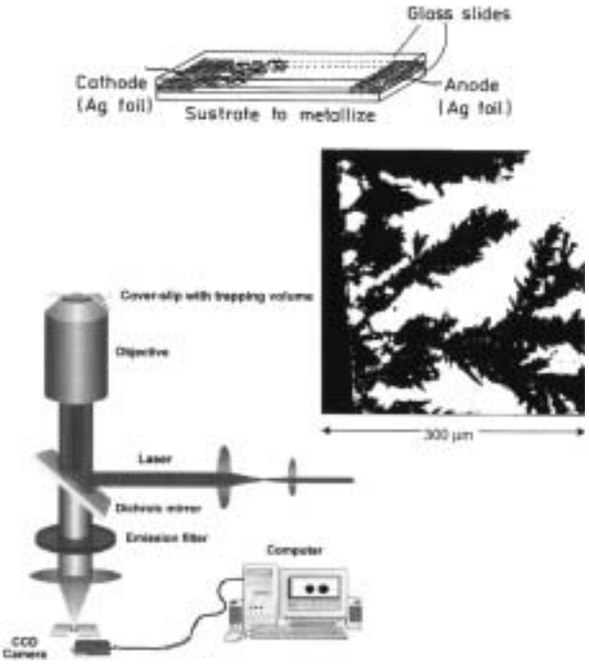

Fig. 5. Top, Configuration for creation of fractal silver surfaces on glass. Right, Silver fractal-like structures on or near the silver cathode. Bright-field image. Bottom, Instrumentation used for observation of silver surfaces and FITC-HSA fluorescence.

reverse start-stop time-correlated single-photon counting). For the FD measurements, excitation was at 514 nm from an argon ion laser, repetition rate of 78 MHz. For TD measurements, vertically polarized excitation at ≈760 nm was obtained using a mode-locked argon-ion pumped, cavity-dumped pyridine 2 dye laser with a 3.77-MHz repetition rate. The instrumental response function, determined using the experimental geometry in Fig. 4 and a glass microscope slide, was typically <50 ps fwhm. The emission was collected at the magic angle (54.7 degrees), using a long pass filter (Edmund Scientific), which cut off wavelengths below 830 nm. This had the effect of showing ICG emission spectra with emission maxima at ≈830 instead of the solution maxima centered near 800 nm. This filter was necessary for roughened silver electrodes so as to discriminate against a highly scattering (reflective) background.

Data Analysis

Both the TD and FD intensity decays were analyzed in terms of the multiexponential model:

$$I(t) = \sum_i \alpha_i \exp(-t/\tau_1) \tag{1}$$

where α_1 are the amplitudes and τ_1 the decay times, $\Sigma\ \alpha_1 = 1.0$. The fractional contribution of each component to the steady-state intensity is given by

$$f_i = \frac{\alpha_i \tau_i}{\sum_j \alpha_j \tau_j} \tag{2}$$

The mean lifetime of the excited state is given by

$$\bar{\tau} = \sum_i f_i \tau_i \tag{3}$$

and the amplitude-weighted lifetime is given by

$$<\tau> = \sum_i \alpha_i \tau_i. \tag{4}$$

The values of α_1 and τ_1 are shown in Table 1. For all the measurements described here, the background was less than 1% from an equivalent sample of silver coating with unlabeled HSA.

RESULTS

Two procedures to produce fractal-like structures were used for metal-enhanced fluorescence, roughened silver

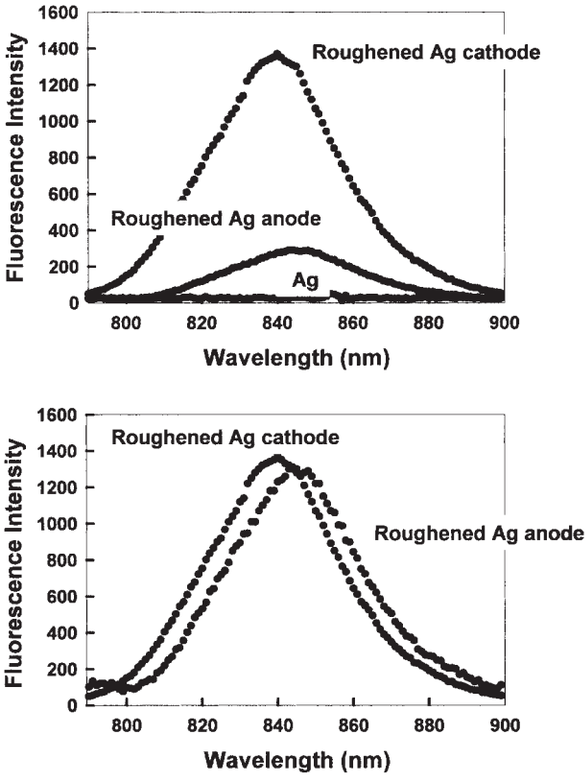

Fig. 6. Top, Fluorescence intensity of HSA-ICG-coated roughened silver electrodes and an unused silver electrode, Ag; Ex = 760 nm. Bottom, Fluorescence intensities normalized to the intensity of the ICG-HSA-coated silver cathode. It should be noted that the normal fluorescence emission maximum (H_2O, pH 7) of 810 nm is shifted in this regard because of the choice of filters that were required to discriminate against a highly scattering silver surface.

electrodes, and the growth of the silver fractal-like structures on glass. Both ICG-and FTIC-labeled protein were used to coat the two structures respectively. We report our findings and compare the merits of both.

Roughened Silver Electrodes

Three electrodes were coated with ICG-HSA and studied, the roughened cathode, the anode, and an unroughened electrode. Essentially no emission was seen from ICG-HSA on an unroughened, bright silver surface (Ag in Fig. 6, the control). However, a dramatically larger signal was observed on the roughened cathode and a somewhat smaller signal was observed on the anode. In all our experiments we typically found that the roughened silver cathode was ≈20–100 fold more fluorescent than the unroughened control Ag electrode. In comparison the Ag anode was 5–50 times more fluorescent than the Ag control. When we increased the time-for-roughening to over 1 h, the intensities of both electrodes after coating with ICG-HSA were essentially the same, but still 50-fold more fluorescent than the unroughened Ag control. The emission spectra on the two electrodes probably had the same emission maximum, where the slight shift seen in Fig. 6 (bottom) is thought to be due to the filters used to reject the scattered light. It should be noted that the amount of material coated on both surfaces was approximately the same, and the effect was not due to an increased surface area and therefore protein coverage on the roughened surface.

The dramatic and favorable increase in fluorescence intensities shown in Fig. 6 could have several explanations. Two possibilities include an increased rate of excitation, due to the enhanced incident fields around the metal [1,2], or increased amounts of protein bound to the fractal structure. For both eventualities the fluorescence lifetimes are expected to remain the same. Examining the intensity decay of ICG-HSA for the cathode we found that the lifetime was dramatically shortened to <10 ps, (Fig. 7), in fact, so short that it was difficult to determine the absolute values with a system time-resolution of ≈50 ps fwhm. However, a decreased lifetime with an increased fluorescence intensity strongly supports an increase in the radiative decay rate [cf. Eq. (3, 4)]. In all our control experiments, scattered light was rejected. For comparison, in buffer the amplitude-weighted lifetime of ICG-HSA was found to be ≈550 ps (Table 1).

ICG is well-known to rapidly degrade in solution because of chemical or photochemical processes. The observed 50–100-fold increases in fluorescence intensity of ICG-HSA seen in Fig. 6 would not be analytically useful if the sample degraded 50–100 times faster. We subsequently examined the steady-state intensity of ICG-HSA

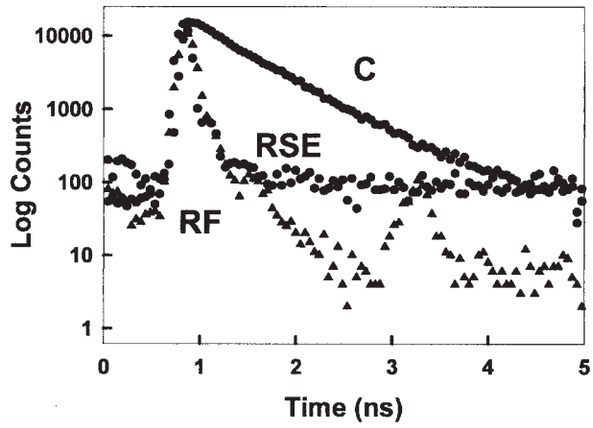

Fig. 7. Complex intensity decays of ICG-HSA in a cuvette (buffer) (C) and on roughed silver electrodes (RSE). RF, Instrumental response function.

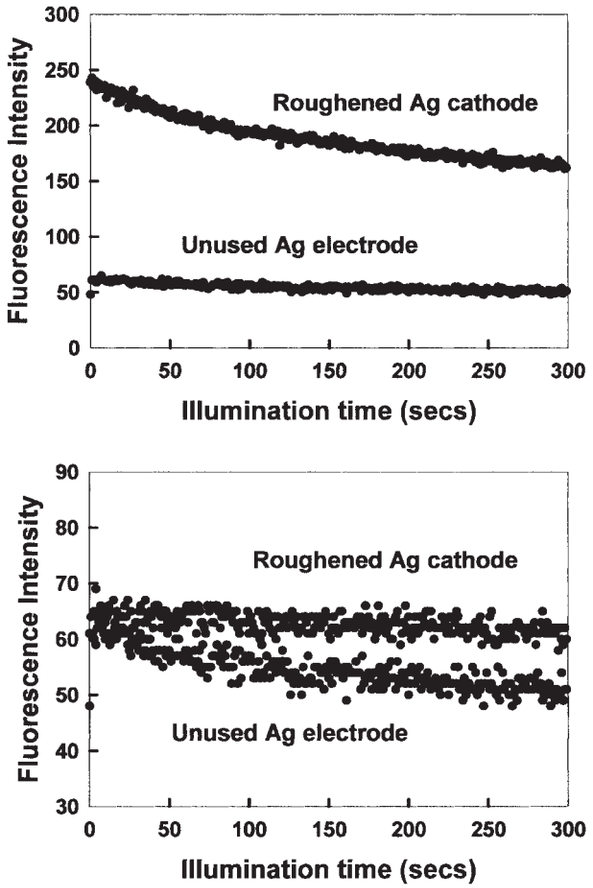

Fig. 8. Top, Photostability of ICG-HSA on a roughened silver electrode and on an unused silver electrode, measured using the same excitation power at 760 nm and (bottom) with the laser power adjusted to give the same initial fluorescence intensities. In all measurements, vertically polarized excitation was used, whilst fluorescence emission was observed at the magic angle, that is 54.7°. It should be noted there is a background of about 40 cps that has not been subtracted in these intensity plots.

with continuous illumination (Fig. 8). At the onset of illumination the relative intensity of ICG-HSA decays more rapidly on the fractal structure than on the control sample (Fig. 8, top). However the effect is small and rates become comparable after 2 min. Interestingly, if the illumination intensity is adjusted so that both samples yield the same steady-state emission intensity at the onset of illumination, then the ICG-HSA on the fractal-like silver cathode photobleaches at a much slower rate (Fig. 8, bottom). Given that the detectable signal from the ICG-HSA is given by the area under these photobleaching curves, then substantially more emission can be obtained from the roughened electrodes compared to the control sample. Intuitively, the ICG intensity remains higher even after the initial decrease in intensity (Fig. 8, top), which suggests that ICG will display higher intensities for longer times when bound to fractal silver electrodes. Such effects are most desirable in many analytical applications such as in high-sensitivity surface assays.

Silver Fractal-like Structures on Glass

For the FITC-HSA-coated fractal-silver surfaces on glass, we were able to measure a fluorescence image very similar to that of the fractal silver surface alone (bright field image) using the same apparatus (Fig. 9 and 10). Interestingly, regions of high and low fluorescence intensity were observed (Fig. 10). This result is roughly consistent with recent SERS data, which showed the presence of intense signals that appeared to be located between clusters of particles [20,21]. Emission spectra were collected from eight selected regions of varying brightness. In all cases, the emission spectra appeared to be that of fluorescein (Fig 10, bottom), where the blue edge of the fluorescein emission is cut off by the emission filter. As a blank control the silver structures were coated with unlabeled HSA. The resulting signal was lower than any of the silvered areas and lower than regions of the unsilvered glass treated with FITC-HSA.

Similarly to the roughened silvered electrodes, we investigated the nature of the enhanced fluorescence intensities observed in Fig. 10 (bottom). If the radiative decay rate is increased, then the lifetime should decrease [1,2]. We measured the frequency-domain intensity decays of FITC-HSA bound to unsilvered glass and fractal silver on glass (Table I). The amplitude-weighted lifetime of FITC-HSA bound to glass is ≈80 ps, which is in agreement with previous measurements of self-quenched fluorescein on HSA [22]. The FITC-HSA sample contained approximately 7 fluorescein molecules per HSA molecule, so that the fluorescein emission was partially quenched by resonance energy transfer (RET) between the fluorophores [22]. On fractal silver, the weighted lifetime is dramatically reduced to about 3 ps. We carefully considered whether this decrease was due to the detection of scattered light. The background signal from unlabeled HSA on fractal silver was less than 1%. The emission filter combination of a 540-nm interference filter and a solution of $CrO_4^{2-}/Cr_2O_7^{2-}$ were selected for low emission from the filter when exposed to scattered light from the sample. However, we do believe a small part of the increased intensity is due to the release of fluorescein self-quenching because of the silver surfaces, but this is estimated to be very small in comparison to the 500-fold increases shown in Fig. 10.

We also studied the photostability of FITC on the fractal silver surface, silver island films (SiFs), and

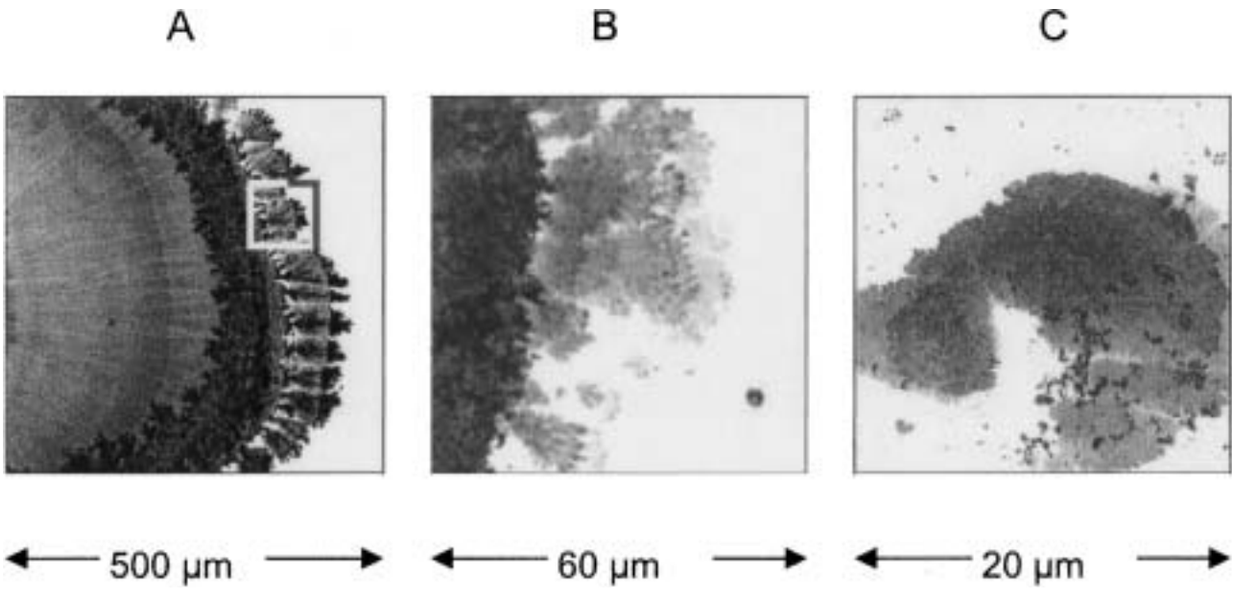

Fig. 9. Silver nanostructures deposited on glass during electroplating (A). Panels B and C are consecutive magnification of the marked area on panel A. Bright-field image.

uncoated quartz. Although the relative photobleaching is higher on fractal silver, the increased rate of photobleaching is less than the increase in intensity (Fig. 11). From the areas under these curves we estimate 16-fold and 160-fold more photons can be detected from the FITC-HSA on SiFs or fractal silver, respectively, relative to quartz, before photobleaching.

Chloride Dipped Electrodes

Finally, to place our work in context with the analytical use of roughened silver electrodes in SERS, we dipped our roughened silver cathode in $10^{-4}M$ chloride for 1 h before coating with ICG-HSA. Such a treatment of the electrode typically results in significantly large enhancements in the surface Raman intensities [16,17]. We questioned what would be observed for the fluorescence intensities. Figure 12 shows the fluorescence intensity of ICG-HSA-coated roughened silver electrode and a chloride-dipped silver electrode under otherwise identical conditions. We generally observed a decrease in the maximum fluorescence intensity of the chloride-dipped electrode compared to the non–chloride-roughened silver electrode. However, the ICG-HSA emission on the chloride-dipped electrode was substantially more fluorescent than on the unroughened electrode. These results therefore suggest that the chloride treatment of the electrodes has no obvious effect on metal-enhanced fluorescence. Our results therefore support current thinking in that SERS is a consequence of surface (near-surface) interactions as compared to metal-enhanced fluorescence, which is considered to be a through-space phenomenon [1,2].

DISCUSSION

In previous papers we have shown that silver particles formed by chemical reduction were effective in increasing fluorescence [1–9]. We have also shown that silver deposited by laser irradiation of a solution of silver nitrate can also enhance fluorescence [8] and the irradiation of electrically produced colloids [9]. The present observation of enhanced fluorescence via fractal structures has some unique advantages not seen with other deposition methods as of yet. One important advantage is the absence of solution reagents such as sodium borohydride or citrate to reduce silver ions to metallic islands. Silver deposition is accomplished in pure water, whilst localization is accomplished by placement of the silver electrodes. Another advantage is that silver can be freshly generated on demand by an electrical current. Producing fractal structures via roughening an electrode requires no preparation of the electrode and no chemical modifications to bind the structures to a surface. Equally as attractive, our second method of silver fractal preparation (see the

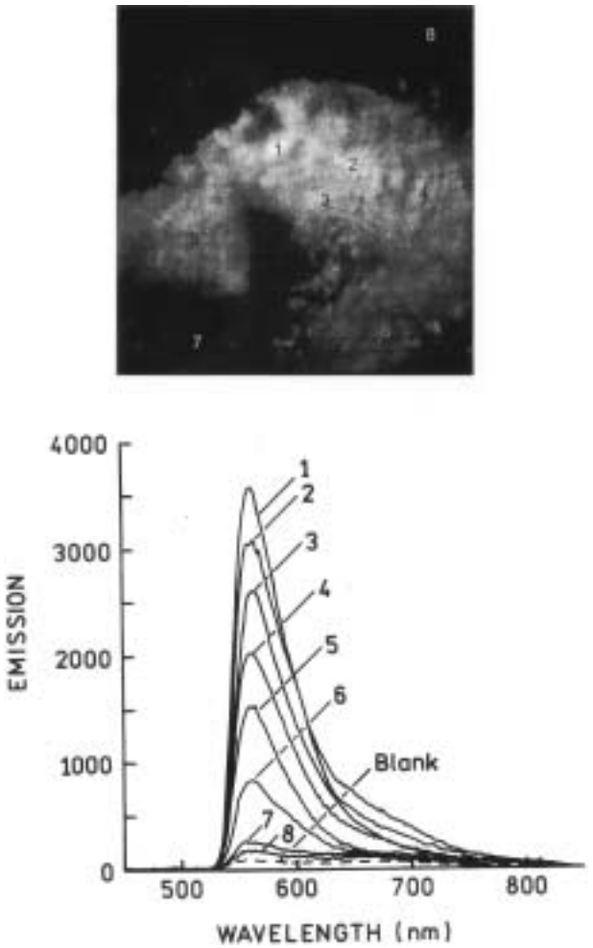

Fig. 10. Top, Fluorescence image of FITC-HSA deposited on the silver structure shown in Fig. 9C. Bottom, Emission spectra of the numbered areas shown above.

discussion of silver fractal-like structures on glass in the Experimental and Results sections) affords for silver structures to be produced from an aqueous medium at neutral pH, which can then bind to a required surface by employing the necessary chemistry. It also appears from our findings that similar fluorescence enhancements can be observed from both silver structures.

The deposition of metallic noble metals on surfaces is presently of intense interest because of the potential applications in nanotechnology. Metal particles can be generated with light [24–26] and by the electroless deposition via galvanic displacement [27]. Additionally, the fractal silver surfaces result in a partial elimination of self-quenching. As a result it will be possible to use these structures with proteins and DNA, which are heavily labeled with fluorophores, as ultra bright reagents for immunoassays or DNA arrays. We envisage that these methods will contribute to the use of metal-enhanced fluorescence in medical diagnostics, biotechnology, and microfluidic and lab-on-a-chip based sensing.

Table I. Analysis of ICG-HSA Measured Using Both the Reverse Start-Stop Time-Correlated Single-Photon Counting (TD) and Frequency Domain Techniques (FD) and the Multiexponential Model

Sample	α_i	τ_I (ns)	f_i	τ (ns)	$<\tau>$ (ns)	χ^2_R
ICG In buffer, (TD)	0.158	0.190	0.05	–	–	
	0.842	0.615	0.95	0.592	0.548	1.4
ICG-HSA Ag cathode* (TD)	1.0	<0.010	1.0	<0.010	<0.010	–
FITC-HSA Glass (FD)	0.907	0.048	0.569			
	0.085	0.242	0.270			
	0.008	1.570	0.161	0.345	0.078	1.5
FITC-HSA Ag fractals (FD)	0.993	0.003	0.854			
	0.007	0.066	0.146	0.012	0.003	1.7

* The roughened Ag cathode had ICG lifetimes <10 ps. With the time-resolution of the system ≈50 ps fwhm, the discrete lifetimes could not be so easily obtained. TD, Time domain; FD, frequency domain.

ACKNOWLEDGMENT

This work was supported by the National Institute of Biomedical Imaging and Bioengineering NIH-EB00682 and the National Center for Research Resource, RR-08119.

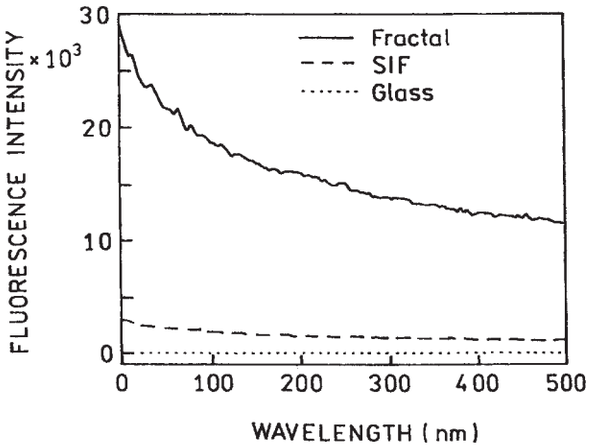

Fig. 11. Photostability of FITC-HSA deposited on glass (····), a silver island film (-----), and fractal silver structures on SnCl2-treated glass (—). The samples were excited at 514 nm.

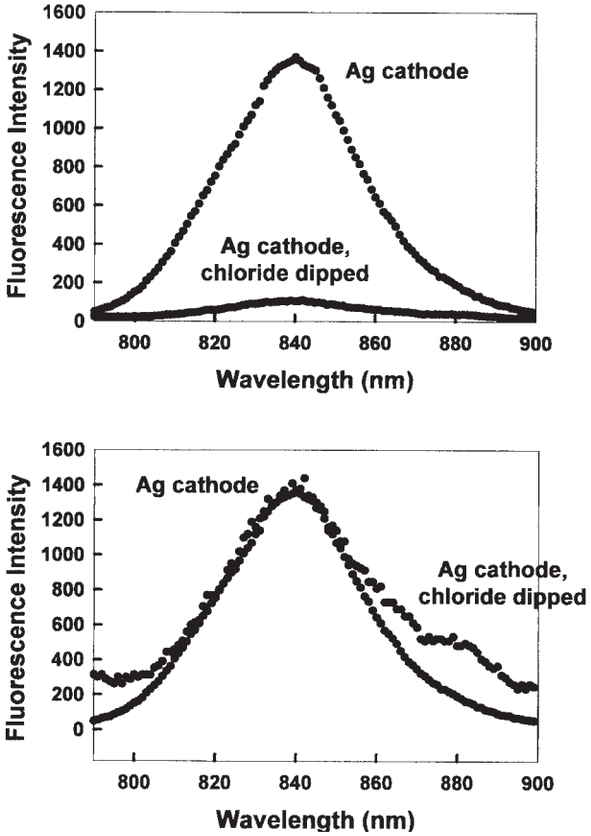

Fig. 12. Top, Fluorescence intensity of ICG-HSA-coated roughened silver electrode and a chloride-dipped silver electrode, Ag, Ex = 760 nm. Bottom, Fluorescence intensities normalized to the intensity of the ICG-HSA-coated silver cathode (no chloride). It should be noted that the normal fluorescence emission maximum (H_2O, pH 7) of 810 nm is shifted in this regard because the choice of filters than were required to discriminate against a highly scattering surface.

REFERENCES

1. C. D. Geddes and J. R. Lakowicz (2002) Metal-enhanced fluorescence. *J. Fluoresc.* **12**(2), 121–129.
2. J. R. Lakowicz (2001) Radiative decay engineering: Biophysical and biomedical applications. *Anal. Biochem.* **298,** 1–24.
3. J. R. Lakowicz, Y. Shen, S. D'Auria, J. Malicka, J. Fang, Z. Gryczynski, and I. Gryczynski (2002) Radiative decay engineering 2: Effects of silver island films on fluorescence intensity lifetimes and resonance energy transfer. *Anal. Biochem.* **301,** 261–277.
4. J. Malicka, I. Gryczynski, J. Kusba, Y. Shen, and J. R. Lakowicz (2002) Effects of metallic silver particles on resonance energy transfer in labeled bovine serum albumin. *Biochem. Biophys. Res. Commun.* **294,** 886–892.
5. C. D. Geddes, H. Cao, I. Gryczynski, Z. Gryczynski, J. Fang, and J. R. Lakowicz (2003) Metal-enhanced fluorescence (MEF) due to silver colloids on a planar surface: Potential applications of indocyanine green to in vivo imaging. *J. Phys. Chem. A* **107,** 3443–3449.
6. J. R. Lakowicz, J. Malicka, I. Gryczynski, Z. Gryczynski, and C. D. Geddes (2003) Radiative decay engineering: The role of photonic mode density in biotechnology. *J. Phys. D* In Press.
7. J. R. Lakowicz, I. Gryczynski, Y. B. Shen, J. Malicka, and Z. Gryczynski, (2001) Intensified fluorescence. *Photonics Spectra* **35**(10), 96–104.
8. C. D. Geddes, A. Parfenov, and J. R. Lakowicz (2003) Photodeposition of silver can result in metal-enhanced fluorescence. *Appl. Spectrosc.* **57,** 526–531.
9. C. D. Geddes, A. Parfenov, D. Roll, J. Fang, and J. R. Lakowicz (2003) Electrochemical and laser deposition of silver for use in metal-enhanced fluorescence. *Langmuir* In Press.
10. N. Christodoulides, M. Tran, P. N. Floriano, M. Rodriguez, A. Goodey, M. Ali, D. Neikirk, and J. T. McDevitt (2002) A microchip-based multianalyte assay system for the assessment of cardiac risk. *Anal. Chem.* **74,** 3030–3036.
11. E. Verpoorte (2002) Microfluidic chips for clinical and forensic analysis. *Electrophoresis* **23,** 677–712.
12. R. Keir, E. Igata, M. Arundell, W. E. Smith, D. Graham, C. McHugh, and J. M Cooper (2002) SERRS: In situ substrate formation and improved detection using microfluidics. *Anal. Chem.* **74**(7), 1503–1508.
13. C. L. Haynes, A. D. McFarland, M. T. Smith, J. C. Hulteen, and R. P. Van Duyne (2002) Angle-resolved nanosphere lithography: Manipulation of nanoparticle size, shape, and interparticle spacing. *J. Phys. Chem. B* **106,** 1898–1902.
14. F. Hua, T. Cui, and Y. Lvov (2002) Lithographic approach to apttern self-assembled nanoparticle multilayers. *Langmuir* **18**, 6712–6715.
15. V. Fleury, W. A. Watters, L. Allam, and T. Devers (2002) Rapid electroplating of insulators. *Nature* **416,** 716–719.
16. M. Fleischmann, P. J. Hendra, and A. J. McQuillan, (1974) Raman spectra of pyridine adsorbed at a silver electrode. *Chem. Phys. Letts.* **26**(2), 163–166.
17. E. Roth, G. A. Hope, D. P. Schweinsberg, W. Kiefer, and P. M. Fredericks, (1993) Simple technique for measuring surface-enhanced fourier transform Raman spectra of organic compounds. *Appl. Spec.* **47**(11), 1794–1800.
18. C. D. Geddes, A. Parfenov, D. Roll, I. Gryczynski, J. Malicka, and J. R. Lakowicz, (2003) Roughened silver electrodes for use in metal-enhanced fluorescence. *Photochem. Photobiol.* Submitted.
19. A. Parfenov, I. Gryczynski, J. Malicka, C. D. Geddes, and J. R. Lakowicz, (2003) Enhanced fluorescence from fluorophores on fractal silver surfaces. *Jn. Phys. Chem. B* In Press.
20. A. M. Michaels, J. Jiang, and L. Brus, (2000) Ag nanocrystal junctions as the site for surface-enhanced Raman scattering of single rhodamine 6G molecules. *J. Phys. Chem. B.* **104,** 11965–11971.
21. A. M. Michaels, M. Nirmal, and L. E. Brus (1999) Surface enhanced Raman spectroscopy of individual rhodamine 6G molecules on large Ag nanocrystals. *J. Am. Chem. Soc.* **121,** 9932–9939.
22. J. R. Lakowicz, J. Malika, S. D'Auria, and I. Gryczynski (2002) Release of self-quenching of fluorescence near metallic surfaces. *Anal. Biochem.* In Press.
23. K. Sokolov, G. Chumanov, and T. M. Cotton (1998) Enhancement of molecular fluorescence near the surface of colloidal metal films. *Anal. Chem.* **70,** 3898–3905.
24. J. P. Abid, A. W. Wark, P. F. Brevet, and H. H. Girault (2002) Preparation of silver nanoparticles in solution from a silver salt by laser irradiation. *Chem. Commun*. **7,** 792–793.
25. E. J. Bjerneld, K. V. G. K. Mutry, J. Prikulis, and M. Kall (2002) Laser-induced growth of Ag nanoparticles from aqueous solutions. *Chem. Phys. Chem*. 116–119.
26. I. Pastoriza-Santos, C. Serra-Rodriguez, and L. M. Liz-Marzan (2000) Self-assembly of silver particle monolayers on glass from Ag+ solutions in DMF. *J. Colloid Interface Sci.* **221,** 236–241.
27. L. A. Porter, H. C. Choi, A. E. Ribbe, and J. M. Buriak (2002) Controlled electroless deposition of noble metal nanoparticles films on germanium surfaces. *Nano. Lett.* **2**(10), 1067–1071.